Research Article

Late Holocene coastal dynamics south of the Chanthaburi estuary, eastern Gulf of Thailand

Armelle Ballian[a,b], Sakonvan Chawchai[c] (ID), Johannes M. Miocic[a,d] (ID), Warinyupa Charoenchatree[c], Raphael Bissen[e] (ID) and Frank Preusser[a] (ID)

[a]Institute of Earth and Environmental Sciences, University of Freiburg, 79104 Freiburg, Germany; [b]Senckenberg Biodiversity and Climate Research Centre, 60325 Frankfurt am Main, Germany; [c]Past and Present Climate Towards the Future (PPCTF) Research Unit, Department of Geology, The Faculty of Science, Chulalongkorn University, Bangkok, 10330 Thailand; [d]Energy and Sustainability Research Institute Groningen, University of Groningen, 9747 AG Groningen, The Netherlands and [e]Department of Mining and Petroleum Engineering, Faculty of Engineering, Chulalongkorn University, Bangkok, 10330 Thailand

Abstract

Beach ridges are depositional features that allow reconstruction of past sea-level variations, sediment dynamics, and storm activity. However, there are still very few systematic studies focusing on beach ridges available from the Gulf of Thailand. Along the east coast, satellite images provide evidence of beach ridges in the Chanthaburi Province, extending as far as 6 km inland, oriented parallel to the current coastline. These can be divided into a set of landward ridges (5.3–6.0 km inland) and seaward ridges (0.4–1.8 km inland) that are separated by an arm of the Chanthaburi estuary. Optically stimulated luminescence dating of 26 sand samples from 12 pits of ridge profiles suggests that the landward set of beach ridges formed ca. 3500 yr ago, while the seaward set of ridges formed between ca. 2100–1200 years ago, which also includes the modern active beach. It appears that the landward set of beach ridges developed during a period of relatively stable sea level followed by a rapid regression presently occupied by the arm of the Chanthaburi estuary. The seaward set of beach ridges apparently reflects a millennium of slowly retreating coastline until the modern beach ridge formed.

INTRODUCTION

Deciphering the response of coastal clastic sedimentary systems to past sea-level changes is important to understanding the potential impact of future developments on these often densely populated areas (e.g., FitzGerald et al., 2008). Sea-level history in coastal settings can be deciphered using a number of proxies (e.g., Lewis et al., 2013), with beach ridge sequences enabling the tracking of sea-level change during post–highstand regression (e.g., Otvos, 2000; Tamura et al., 2012). Hence, beach ridge systems, characterised by parallel to subparallel ridges and swale topography, are prominent features reflecting longer periods of costal development. While there has been discussion since Davies (1957) regarding the exact processes that lead to the formation of beach ridges (cf. Tamura, 2012; Kelsey, 2015; Oliver et al., 2017), it is agreed that ridge formation is mainly influenced by changes in sea level, local wave/tide conditions, storminess, gradient, and the degree of sediment supply. Commonly, it is expected that relative sea level (RSL) rise will erode and move beach ridges towards a more landward equilibrium position, whereas beach ridge plains prograde seaward during sea-level fall (Hansom, 2001; Plater and Kirby, 2011). However, the exact controlling factors, mechanisms, and timing remain poorly understood (e.g., Tamura, 2012).

A key method to quantify process rates is determining the age of coastal features, using radiocarbon dating and/or optically stimulated luminescence (OSL) dating (e.g., Jacobs, 2008). Applying different combinations of geomorphic analyses, geophysical surveying, sedimentary investigations, and geochronological approaches and identifying sea-level indicators have been used to reconstruct long-term coastal dynamics in numerous case studies. However, these concentrate on the midlatitudes, in particular along the sandy coasts of Australia (e.g., Short and Hesp, 1982; Oliver et al., 2015), North America (e.g., Mallinson et al., 2008; Shawler et al., 2021), and Europe (e.g., Faye et al. 2019; Nielsen et al. 2006). In contrast, the number of comprehensive and systematic studies using a combination of at least several of the abovementioned methods in Southeast (SE) Asia is still rather low (e.g., Hanebuth et al., 2011; Mallinson et al., 2014; Brill et al., 2015; Gouramanis et al., 2020; Kongsen et al., 2022). In particular, age control of deposition is often limited to a rather low number of radiocarbon and/or OSL samples.

Presented here is a study of coastal features along the southern edge of the Chanthaburi estuary, located ca. 245 km southeast of
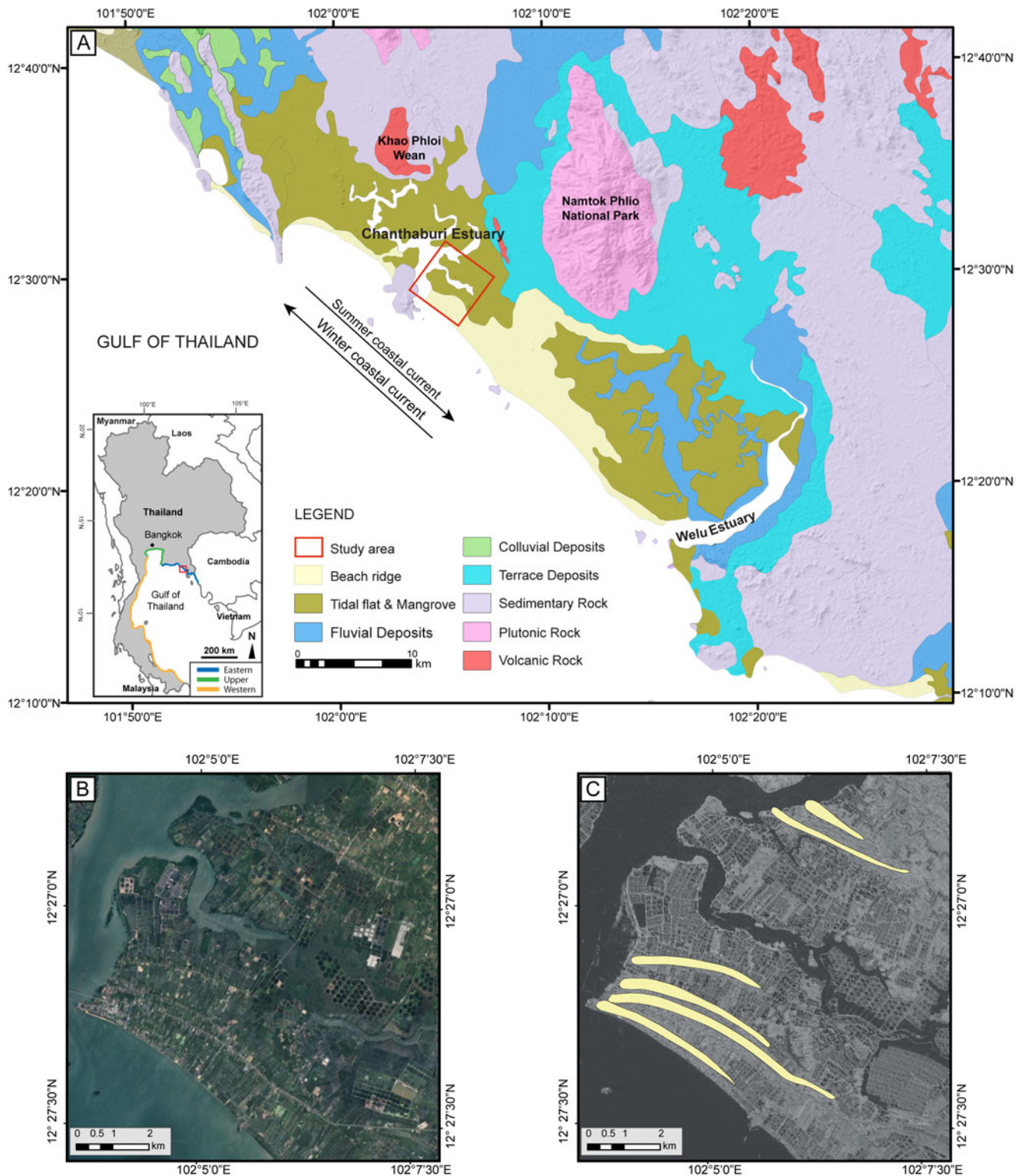
Figure 1. (A) Geomorphologic and geologic map of the Chanthaburi area, eastern Gulf of Thailand (study area indicated by the red rectangle). Inset: location of the study area in the Gulf of Thailand (DMR, 2007, 2001). (B) Satellite imagery of the study area and (C) beach ridges studied indicated on the TanDEM-X digital surface model.

Bangkok (Fig. 1), aimed at identifying the timing and discussing potential processes that shaped the present coastal landscape. To do so, we first apply a combination of geomorphologic mapping of ridges found parallel to the coast and then investigate sedimentary features in trenches hand-dug into the ridges to identify the local facies. A major focus is on establishing reliable age constraints of coastal evolution by using OSL dating on samples taken from the trenches. The results will be used to reconstruct the Late Holocene history of the coast strip and discuss it in a regional context.

REGIONAL SETTING

Past and modern sea-level change in SE Asia

The Gulf of Thailand is located on the continental shelf of the South China Sea and is divided into eastern, upper, and western parts (Fig. 1). In this region, sea level may rise as much as 60 cm until the end of the twenty-first century (Oppenheimer et al., 2019), depending on the global warming scenario used for simulations (Jaroenongard et al., 2021). Such predictions are supported by tide gauge data (Sojisuporn et al., 2013) revealing a sea-level increase of about 5 mm/yr for the period AD 1985–AD 2009, in a similar range as altimetry measurements (Trisirisatayawong et al., 2011). For the Sunda Shelf somewhat farther south, Culver et al. (2015) reconstruct an increase in the rate of sea-level rise from 1.26 mm/yr for the period AD 1820–AD 1900 using radiocarbon dates of peat to about of 3.2 ± 0.6 mm/yr for the last 120 yr based on foraminiferal data. This highlights the need to understand the timing of coastal sedimentary processes in the region in the light of future sea-level rise.

On Holocene time scales, RSL changes in SE Asia resulted from a combination of eustatic, isostatic, and local factors such as human-induced subsidence and sediment supply (e.g., Kengkoom, 1992; Sinsakul, 1992; Tjia, 1996; Scoffin and Le Tissier, 1998; Horton et al., 2005; Oliver and Terry, 2019; Durand et al., 2022). For example, a Holocene maximum of +2.6 m at ca. 5.7 ka was inferred based on oyster and coral data from Phang-nga Bay and Phuket, whereas ridge crests and swale bases in the northwest of the Andaman Sea coast (Phuket) point to maximum heights of +1.5–2.0 m above present sea level around 5.3 ka (Scheffers et al., 2012). According to this study, RSL in the region did not exceed +1.5 m during the last 3000 yr. Mann et al. (2019) provide a standardized Holocene RSL database for SE Asia, the Maldives, India, and Sri Lanka. Overall, geomorphic evidence reveals a rise of RSL from below −30 m during the Early Holocene (12–8 ka) reaching a higher than present RSL between 6 ka and 4 ka, with amplitudes between 2 and 5 m above mean sea level. After 4 ka, RSL has been falling and likely reached the present height during the past two millennia (Mann et al., 2019). Interestingly, Mann et al. (2019) combine evidence from the northern Gulf of Thailand with the South China Sea, in particular the Mekong Delta, and observe an ambiguous age-elevation of RSL change in the available data. It should be noted that Mann et al. (2019) rely on and critically access rather old data from the northern Gulf of Thailand (Somboon, 1988; Somboon and Thiramongkol, 1992) that were published with very limited information with regard to exact sample location and no information regarding dating procedures. Nimnate et al. (2015) discuss several sea-level reconstruction curves stretching from Singapore to the northern Gulf of Thailand, revealing large differences in the peak and shape of Holocene sea-level rise and fall (Sinsakul et al., 1985; Hesp et al., 1998; Choowong 2002a; Horton et al., 2005). These authors also present a revised sea-level curve based on OSL data from beach ridges at Chumphon, Gulf of Thailand that implies a maximum RSL of more than 4 m around 7–6 ka, followed by a gradual decrease and reaching the present level after 2 ka. However, the elevation data of Nimnate et al. (2015) might be inaccurate and overestimated (Choowong, M., personal communication, 2023). Surakiatchai et al. (2019) revise the sea-level curve from the Prachuap Khiri Khan beach ridge plain and find good agreement with the ICE-5 G sea-level model (Peltier, 2004), with a peak sea-level elevation of ca. +3 m between ca. 8 and 7 ka.

Study area

The study area is located within the Laem Sing District, Chanthaburi Province, in the coastal area south of the Chanthaburi estuary (Fig. 1). A similar setting is found ca. 30 km southeast, along the Welu estuary (Chataro et al., 2022). Based on the geomorphologic and geologic maps from the Department of Mineral Resources of Thailand (DMR 2001, 2007), the research area features beach ridges, tidal flats, fluvial deposits, terrace deposits, colluvial deposits, sedimentary rocks, plutonic rocks, and volcanic rocks (Fig. 1). Granitic rocks are widely distributed in Thailand and occur in eastern, central, and western granite belts (Charusiri et al., 1993), with the Chanthaburi granitic rock being a coarse-grained biotite granite (Uchida et al., 2022). Along with the granitic rocks, Carboniferous–Triassic shallow- to deep-marine sedimentary rocks and Quaternary alluvium are widely dispersed in the study area (Sone et al., 2012). Neogene to Quaternary intraplate basalt occurs locally (Fig.1).

The geologic setting results from the fact that Thailand underwent extensive deformation during the late Mesozoic/early Cenozoic due to the collision of the Indian and Eurasian terranes. This was associated with sinistral strike-slip faults also common within the Sa Kaeo–Chanthaburi Zone, representing the likely origin of NW-SE trending geologic structures (Sone et al., 2012; Hara et al., 2018). In the eastern Gulf of Thailand, rifting began in the Eocene and ended at the Oligocene–Miocene boundary (Phoosongsee and Morely, 2019). Since the late Miocene, the coastal area of the eastern Gulf of Thailand is considered tectonically stable (Choowong, 2002a), and no seismic risk is expected for this region (Pailoplee and Choowong, 2013; Pailoplee and Charusiri, 2017), indicating the lack of active tectonics.

The coastal regions of the northern Gulf of Thailand have kept a record of their evolution, particularly in relation to how they responded to the sea-level changes during the Holocene. A first framework combining geomorphic evidence and sedimentary facies evolution was presented by Choowong (2002b) and later refined using both radiocarbon and OSL dating (e.g., Nimnate et al., 2015; Surakiatchai et al., 2018, 2019; Chataro et al., 2022; Miocic et al., 2022). In the eastern Gulf of Thailand, several tide-dominated estuaries populate the coastline; they are located in sheltered areas between protruding headlands, protected from high wave energy (Choowong, 2002a). Minor sea-level fluctuations during the postglacial marine transgression that caused the rapid flooding of the Sunda Shelf (Hanebuth et al., 2000) affected the evolution of the sedimentary sequences (transgressive, aggregational, and progradational or regressive facies) and continued to develop until the Late Holocene (Choowong, 2002a, 2002b).

The lower part of Laem Sing District is characterized by coastal plains interspersed with hills and tidal flats. Chanthaburi Province has the largest mangrove areas in eastern Thailand, occupying ca. 60% of the coastal plain. Mangrove forests are located in sheltered coastline and inland areas, along the banks of rivers and streams (Suk-ueng et al., 2013). The Chanthaburi and Welu are the two major rivers in the Chanthaburi and Trat Provinces, respectively.

The Chanthaburi River (approximately 120 km long) originates in the northern mountains (Khao Ploi Waen, basalt, granitic basement), flows through Chanthaburi city, and finally empties into the Gulf of Thailand in the Laem Sing District. For the research area, there are no statistics on annual runoff or sediment discharge available. However, the runoff of the Chanthaburi River is substantially less than that of the Welu River (Chen et al., 2020).

Because of its narrower channel, the Chanthaburi estuary is less vulnerable to seawater intrusion than the Welu estuary, which is invaded by salt water during high tide (Chen et al., 2020).

Sediments at the mouths of the Chanthaburi estuary and the Welu estuary fluctuate under the influence of tidal currents and are considered strongly hydrodynamic (Wang et al., 2020), with the areas of highest sand content found in the southwestern Chanthaburi estuary. The Chanthaburi estuary also has a more complicated sand volume fraction than the Welu estuary, as the sand content at the mouth is higher and shows an outward extension with a gradual reduction in sand content (Wang et al., 2020). The sand volume fraction gradually decreases with distance offshore under the influence of the tidal current. The tides in the study area are diurnal, with an average tidal range of 0.8–1.2 m (Chen et al., 2020; Trisirisatayawong et al., 2011).

The Indian summer monsoon (SW monsoon) and the northeast winter monsoon (NE monsoon) define the present-day climate in the region. Thus, seasonal variations in the dominant wind directions have a significant impact on wind-driven currents in the Gulf of Thailand. In the summer, during the SW monsoon, currents flow in a clockwise direction (Fig. 1). While the currents remain generally clockwise during the NE monsoon, they are counterclockwise in the eastern part of the gulf (Chen et al., 2020; Liu et al., 2016; Wang et al., 2020). During the winter, a westward-directed current flows along the coast of the study area; tides are diurnal, with an average tidal range of 0.8–1.2 m (Chen et al., 2020; Trisirisatayawong et al., 2011).

During the summer season, as a result of overheating, low-pressure weather systems form in the tropics; these cyclones generally move from east to west. Due to its location, the Gulf of Thailand is exposed to such tropical storms, but the most and the strongest of those hit the eastern coast of the Thai-Malay Peninsula, mainly between 8°N and 12°N (Terry et al., 2018). During the period 1952–2020, a total of 36 tropical cyclones passing the Gulf of Thailand also affected eastern Thailand, mainly during September and October (Thai Meteorological Department, 2020; Supplementary Table S1). However, only nine of those had a substantial impact on the Chanthaburi coast, namely those occurring in July 1951 and in the October of the years 1952 (twice), 1957, 1959, 1960, 1974, 1985, and 1992 (Thai Meteorological Department, 2020).

METHODS

Geomorphology

Satellite images, digital elevation models (DEMs; TanDEM-X with 12 m horizontal and <1 m vertical resolution), and a geomorphologic map (DMR, 2001) were used to classify landforms in the study area and identify suitable sampling locations. Twelve locations along two transects perpendicular to the recent shoreline were selected for field observations (Fig. 2). During site selection, special focus was put on areas with limited or no visible human impact. Following hand auger probing, small trenches with a depth of 1.0–1.5 m were excavated at each location, with the groundwater table limiting the depth of the trenches. Pürckhauer probing allowed for sedimentologic observations beneath the ground water table. The clean trench walls were photographed and logged, and the exact location of each trench was determined using differential GPS (dGPS; ±5 cm in height). To confirm field estimates, 22 samples were taken from areas of interest for sedimentologic analyses (grain-size analysis,

organic and carbonate content). The profile illustrated in Figure 2 is based on a combination of remote sensing data and field data (TanDEM-X, dGPS, geomorphologic observations).

Sedimentology

Sedimentologic samples were homogenized and dried at 105°C for 24 h. Organic matter and carbonate content of the samples were analysed by loss on ignition (LOI; Heiri et al., 2001; Santisteban et al., 2004) using a muffle furnace with temperatures of 550°C for 3 h for organic matter and 950°C for 2 h for carbonate content. For laser-optical grain-size analysis, the fraction >2 mm (if present) was removed by sieving, and the remaining material was pretreated with 20% H_2O_2 at 70°C for organic matter degradation. As the detrital grains partly consist of carbonate fragments, the samples were not treated with HCl before grain-size analysis. The samples were then treated with a dispersant (Calgon, a solution of 33 g sodium-hexametaphosphate, and 7 g sodium carbonate) for 24 h (Abdulkarim et al., 2021) before grain-size distribution was analysed with a Malvern Mastersizer 3000. Grain-size data were analysed using GRADISTAT (Blott and Pye, 2001) (Supplementary Table S2).

Luminescence dating

For OSL dating, 26 samples were collected by forcing a 10-cm-diameter iron cylinder horizontally into the cleaned section at depths of more than 40 cm to avoid potential bioturbation. To avoid depleting the OSL signal, samples were taken without exposure to daylight. Samples were therefore immediately packed from the cylinder into opaque plastic bags. Thereafter, additional sediment was collected in a 30 cm radius around the OSL sample for dose-rate determination. The initial part of the sample preparation work was done at the red-light laboratory at Chulalongkorn University, Bangkok. First, the water content was measured, and samples were subsequently dry sieved (105–177 μm); this was followed by removal of carbonate and organic material using HCl and H_2O_2, respectively. Heavy minerals were removed using a magnetic separator. The samples were then transferred to the University of Freiburg, where they were etched using 40% hydrofluoric acid for 1 h to remove the outer layer of the mineral surface that is affected by alpha radiation. Dried grains were mounted on stainless steel discs using a 2 mm stamp of silicon oil (ca. 50 grains per aliquot).

Luminescence measurements were performed on an automated TL/OSL-DA-15 Risø reader fitted with a bialkali EMI photomultiplier. The $^{90}Sr/^{90}Y$ beta source of the reader was calibrated using LexCal2014 calibration quartz (90–160 μm; 3 Gy administered dose) to ca. 0.11 Gy/s. Equivalent dose (D_e) measurements were carried out using a modified version of the single-aliquot regenerative-dose protocol (SAR) of Murray and Wintle (2000), with preheating at 230°C for 10 s before all optical stimulation, as identified appropriate in performance tests (dose recovery, thermal transfer, preheat plateau). Most of the samples show bright OSL signals and an excellent response during the SAR protocol (Supplementary Fig. S1). Twenty-four replicate measurements were considered sufficient for most samples. However, for six of the very young samples (less than 100 yr old) the number of replicate measurements was increased to 30. For several samples, some aliquots had to be rejected due to poor quartz luminescence sensitivity or not passing the SAR quality criteria (recycling ratio within 10% of unity, test dose error <10%). D_e calculation was conducted based on either the central age model (CAM) or the minimum age
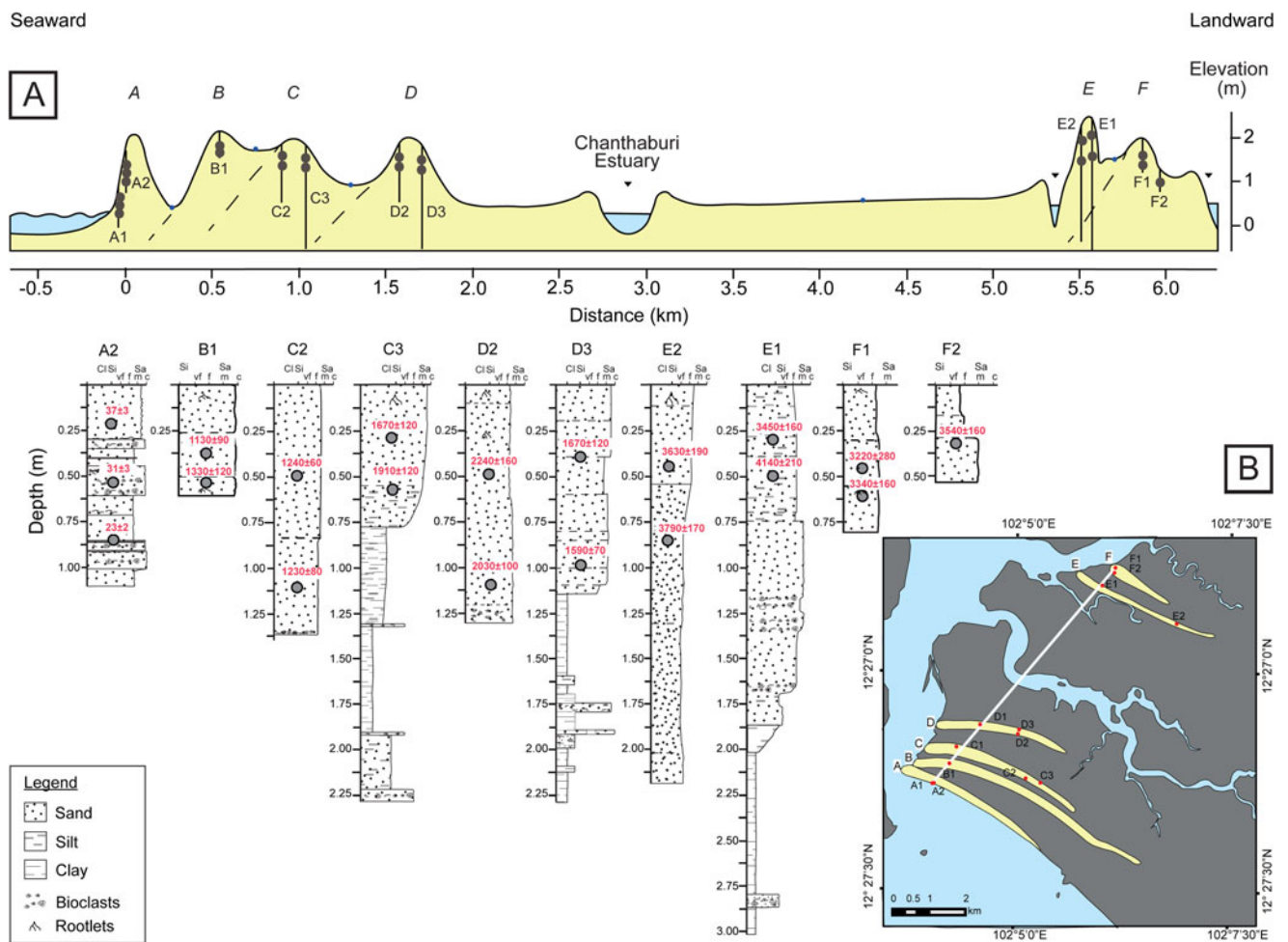
Figure 2. (A) Cross section through the studied beach ridges along the line indicated in B. (B) Simplified geomorphologic map of the study area showing the sampling locations.

model (logged MAM-3; Galbraith et al., 1999). The determination of the appropriate age model was based on the shape of the D_e distribution and the observed overdispersion. A sigma_b value of 0.10 was used in the MAM calculations.

The determination of the concentration dose-rate relevant elements (K, Th, U) was carried out at VKTA (Radiation Protection, Analytics & Disposal Rossendorf Inc.) in Dresden, using high-resolution gamma spectrometry (cf. Preusser and Kasper, 2001). No evidence for radioactive disequilibrium in the uranium decay chain was observed. Dose rates and ages were calculated using the software ADELE v. 2017 (Degering and Degering, 2020; www.add-ideas.de). Cosmic-ray dose rates were corrected for geographic position and burial depth after Prescott and Hutton (1994). All luminescence data are summarised in Supplementary Table S3. Mean ages used in the discussion are based on the CAM of OSL individual ages, as this approach represents a geometric mean and includes the individual uncertainties in the calculations.

RESULTS

Geomorphology

Based on geomorphologic analysis of remote sensing data, two series of former beach ridges were recognized in the study area

(Fig. 2). This comprises a series of four closely spaced ridges (A–D) near the shore of Leam Sing beach, and a second set including two main ridges (E and F) and a nonprominent subridge, also closely spaced, several kilometres farther inland. All ridges reach a height of about 1–2 m above the neighbouring plain, which is about 0.5 m above present-day sea level. While ridges were to some extent modified by human activity, their individual overall morphology and dimension are still clearly identifiable on satellite images. Furthermore, from field observations, it is concluded that human modifications appear rather limited and will not have significantly disturbed the overall geomorphic setting.

Beach ridge A, located at the shore of the Gulf of Thailand, is the longest, with a length of about 7 km and a width ranging from 115 to 280 m. Farther inland, the widest ridge, B (5.1 km long and up to 350 m wide), is easily identified by a road being constructed on its crest. The following ridge, C, is less elongated (2.4 km long) but has about the same width. Ridge D is slightly longer (2.8 km) but with a smaller width (175 m) and a more convex shape. The second set of ridges is separated from the first by a 3.5-km-wide estuary channel system and contiguous low-lying areas. The seaward-facing ridge of this set, ridge E, has a length of 3 km and a width of 195 m. The most landward ridge of the study area (ridge F) has a length of 1.9 km and width of up to 190 m.

Sedimentology

The ridges are composed of sand beds with the thicknesses of individual beds ranging from 5 to 70 cm, which overlie finer-grained sediments (Fig. 2). The overall thickness of the individual sand ridges ranges from 0.75 m to more than 2 m. The sand beds contain predominantly fine to medium, poorly to moderately sorted sand with a low organic content (<1.6%). Carbonate content is generally low (< 2%); however, coarse, bioclast-rich layers are common. Bedding structures are generally only visible due to grain-size changes, while internal structures in individual sand beds are usually not visible in the pits. Detailed sedimentologic descriptions of all pits, as well as images, are found in the Supplementary Material. Generally, the topmost 10–20 cm of each sedimentary sequence is organic rich and shows clear signs of soil formation. The underlying sands are featureless, grey to dark grey. In all locations, the colour changes to orange reddish with depth, indicating an oxidizing environment.

The following summary of sedimentologic observations will concentrate on the main transect of the study. At the recent beach ridge, A, the foreshore (A1; Supplementary Fig. S3) shows structureless sands with a thickness of at least 1.1 m. At the backshore (A2; Supplementary Fig. S4), sedimentary structures are well preserved, featuring erosional unconformities at the base of cross-bedded, poorly to moderately sorted, bioclast-rich, medium to coarse sand beds. Interbedded with these beds are moderately to well-sorted, laminated fine sands. At ridge B (Supplementary Fig. S5), poorly sorted sands have a thickness of at least 0.6 m, while the seaward side of ridge C (C2; Supplementary Fig. S6) consists of poorly to moderately sorted, featureless, fine to medium sands with an overall thickness of at least 1.35 m. At the base of the pit, one bioclast-rich layer occurs. Landward (C3; Supplementary Fig. S7), the sands have an overall thickness of ~0.8 m, and the underlying clayey silts and clays feature interbedded coarser, bioclast-rich layers. On the seaward side, Ridge D (D2; Supplementary Fig. S8) consists of fine to medium sands that are moderately to poorly sorted and are at least 1.3 m thick. One bioclast-rich layer is present and fining upward trends within laminae are observed. On the landward side (D3; Supplementary Fig. S9), stacked fine to medium sands up to 1.15 m depth are present, with dark grey clays beneath, with several interbedded, poorly sorted, bioclast-rich sandy layers.

The upper ca. 1 m of the inland ridges (E and F) are composed of fine to medium, moderately to poorly sorted, partly silty sand. On the seaward side of ridge E (E2; Supplementary Fig. S10) the sands are at least 2.2 m thick, commonly poorly sorted, and silty, with some coarsening upward trends within laminae being visible. No bioclast-rich layers are observed. On the landward side of ridge E (E1; Supplementary Fig. S11), the sand beds have an overall thickness of 1.9 m, and there are at least three ca. 10-cm-thick, poorly sorted, bioclast-rich beds. Below 1.9 m depth, greyish clays dominate, with one poorly sorted, bioclast-rich sandy silt layer occurring at 2.8 m depth. The fine to medium, moderately to poorly sorted sands of ridge F have an overall thickness of at least 0.8 m (F1; Supplementary Fig. S12) and 0.55 m (F2; Supplementary Fig. S13) on the sea- and landward sides, respectively. No bioclast-rich layers are observed in ridge F; however, this could be due to the shallow depth of the pit on the landward side.

LOI-based organic matter content (0.13–1.53%) and carbonate content (0.05–1.89%) of the analysed samples show no consistent trends with respect to sample location (landward vs. seaward side of the ridges) or depth (Supplementary Table S2). Samples with a high organic matter content tend to be shallow and are interpreted to have been subject to soil formation processes, while samples with a high carbonate content visibly contain shell fragments.

Results from the grain-size analysis indicate no obvious trend in the overall distribution of the sediments from ridges A to F. Most of the sediments are moderately to poorly sorted, with sorting ranging mostly from near symmetrical to fine-skewed, as well as ranging widely between mesokurtic and very leptokurtic. However, the distribution of sediments from the most landward ridge (F) differs significantly from the others regarding kurtosis and skewness value variations (Supplementary Fig. S2).

Deposition chronology

OSL ages of samples from the present beach ridge were taken from a structureless forebeach setting (A1) and a well-stratified backshore (A2) section. For both settings, OSL ages in the order of decades have been determined (from bottom to top: A1, 32 ± 3 yr, 43 ± 5 yr, 32 ± 3 yr; A2, 23 ± 2 yr, 31 ± 3 yr, 37 ± 3 yr). While the ages are not strictly consistent within the given 1-sigma uncertainties, it is interesting to note that the D_e values are similar (Supplementary Table S3). Hence, the slight inconsistencies might rather be related to dose-rate issues, a problem already highlighted and discussed in a similar setting by Miocic et al. (2022). Nevertheless, it appears justifiable to infer an age of some 30 yr for the deposits.

The OSL ages determined for the seaward beach ridge complex (B–D) increase landward with no systematic increase of age with depth in the individual profiles. For the most seaward position (B1: ages of 1130 ± 90 yr and 1330 ± 120 yr), this represents a mean age of ca. 1210 ± 70 yr. The next landward position gave ages (C2: 1230 ± 80 yr, 1240 ± 60 yr) very consistent with this estimate, with a mean of 1240 ± 40 yr. However, the landward side of this beach ridge shows higher ages of 1910 ± 160 yr (C1) as well as 1910 ± 120 yr and 1670 ± 120 yr (C3) (mean = 1800 ± 90 yr). This trend continues on the seaward side of the next beach ridge (D2: 2030 ± 100 yr, 2240 ± 160 yr), with a mean of 2100 ± 80 yr. Interestingly, the landward side of this ridge (D3: 1590 ± 70 yr, 1670 ± 120 yr) shows a significantly lower mean age of 1610 ± 60 yr. Striking for this beach ridge is the difference in dose rate, which is just above 0.5 Gy/ka on the seaward side, but around 1 Gy/ka on the landward side. This is caused by a higher concentration of all dose rate– relevant elements (K, U, Th). We speculate that the sediment on the landward side might be less weathered and hence represents a more prominent contribution of fresh material provided by the Chanthaburi River. Therefore, it appears possible that this side of the beach ridge was not overprinted by direct marine processes, but by fluvio-estuarine influence. It might indeed represent a young aggradation of sediment, for example, a reworking by tidal processes on the landward compared with the seaward side. OSL ages determined for D1 (370 ± 60 yr, 1020 ± 120 yr) are inconsistent with all other ages. We later learned that this area might have been subject to land fill operations and hence excluded the results in the "Discussion."

The OSL ages determined for the landward beach ridge complex (E and F) all overlap within uncertainties, with the exception of sample CHA12Q (4140 ± 210 yr). The results show no correlation with older ages being more landward (Fig. 2) and represent a mean of 3530 ± 70 yr.

DISCUSSION

While the Chanthaburi coastal plain is topographically flat, ridges are clearly visible, with elevations up to 4 m above present mean sea level in the DEM. However, due to limitations in the vertical resolution, the DEM data cannot be used to create a reliable detailed elevation profile across the transect. Note that the ridges have been altered by human activity, as they serve as urban areas, whereas the area between the ridges is commonly used for fish farming. Compared with an earlier mapping of barriers and ridges by Choowong (2002b), our results seem to be more accurate and detailed, while the general setting and locations are similar. The higher level of detail is explained by the increased quality of the remote sensing data being used. The ridges are interpreted to be beach ridges outlining past shorelines, indicating that five palaeo-shorelines are recorded (ridges B–F) in addition to the recent shoreline (ridge A). Noteworthy is the gap between the two sets of beach ridges, which is currently occupied by one arm of the Chanthaburi estuary.

The analysis of the grain-size distribution parameters and their correlations does not allow identification of any depositional process of the different units (Supplementary Fig. S2). However, grain-size parameters of ridge F, which is located most landward, differ significantly from the other ridges and the sediments are very coarse skewed and very leptokurtic. This implies that sediments of ridge F were deposited under different hydrodynamic conditions than the rest of the ridges.

A general lack of sedimentary structures does not allow for a detailed interpretation of depositional processes; however, the sand beds at the tops of the ridges are interpreted to be the result of wave and aeolian deposition in a beach environment as observed at the currently active beach ridge. The nature of the backshore environment is well documented in the recent beach site, where bioclast-free laminated sands are interbedded with cross-bedded bioclast-rich coarse sands. The laminated sands represent the normal deposition due to wave action in the swash zone and reworking of these deposits by aeolian processes. The poorly sorted bioclast-rich layers in A2 are interpreted to represent a storm event, where material from below the mean fair-weather wave base has been transported to the beach and deposited there. Considering that the coast of Chanthaburi is quite infrequently hit by major storms and given the OSL age of ca. 30 yr, Typhoons Gay (AD 1989) and Linda (AD 1997) are the most plausible candidates. Regarding the latter, a possible slight overestimation of the age due to potential partial bleaching should be considered. The average wave height during Typhoon Linda along the eastern coast of Thailand was about 2.5 m, with a maximum storm surge height of 0.6–1.0 m generated in the upper Gulf of Thailand (Vongvisessomjai, 2009). Typhoon Gay, approaching from the South China Sea, generated a maximum wave height of 6–11 m, with storm surge heights that might have reached 2 m height. In the past, storm events with such intensity are evident on the landward side of the ridges, where bioclast-rich, poorly sorted layers are commonly found (ridges C–E). The storms must have had such an intensity that waves swept over the crests of the ridges.

The seaward-facing sections of ridges B–E likely represent the aeolian-wave interaction occurring on the foreshore, as the clear laminations and cross stratifications observed in the recent swash zone deposits are missing. The moderate to poor sorting of these sands excludes pure aeolian processes; however, the lack of frequent storm indicators may highlight that they were deposited higher than the mean storm level on the ridge.

The silty and clayey sediments occurring beneath the sands (ridges C–E) are interpreted to represent tidal flat deposits. Their fine-grained nature is likely linked to the proximity of the Chanthaburi estuary, which delivers fine-grained sediments into the Gulf of Thailand. Coarse-grained, bioclast-rich layers within these sediments are interpreted to be the result of strong storm events.

According to OSL dating, the landward set of beach ridges (E and F) was formed ca. 3500 yr ago, some 6 km inland from the current shoreline at the Chanthaburi estuary. Coastal landforms several kilometres inland with similar OSL ages have been reported from the western Gulf of Thailand, at Sam Roi Yot National Park (ca. 200 km W of the study area; Surakiatchai et al., 2019), as well as from the eastern Gulf of Thailand, from sand spits at the Weru estuary (ca. 25 km SE of the study area; Surakiatchai et al., 2019), and from the Trat Province (ca. 70 km SE of the study area; Chataro et al., 2022). In summary, there is clear evidence for a coastline retreat in several parts of the northern Gulf of Thailand in the past 3500 yr that reaches a distance of several kilometres (Fig. 3A).

The most common explanation of widespread coastline retreat is the lowering of the regional sea level. Indeed, sea-level data from SE Asia point towards about 1.5–2.5 m sea-level lowering during this time (Scheffers et al., 2012; Stattegger et al., 2013; Oliver and Terry, 2019; Surakiatchai et al., 2019). However, the question remains whether other factors contributed to this relocation of the coastline. Increased storminess would likely have led to erosion of the beach ridges and a rather transgressive trend of the coastline. An increase in sediment supply and/or decreased storminess would likely have caused a continuous aggradation of beach ridges, as observed by, for example, Oliver et al. (2020) in southern Australia and Rodrigues et al. (2022) in Florida. The fact that the next set of beach ridges is located some 3 km seaward speaks against continuous aggradation. However, a lack of deposition could also be related to a decrease in sediment supply, so beach ridges might never have formed in this zone, or previously existing beach ridges might have later eroded. Interestingly, Chataro et al. (2022) also recognised a gap in beach ridge formation at Pailin Beach (70 km SE of Chanthaburi) between ca. 3000 and 1800 yr in a spatially close setting. While the amount of data is very limited, the coincidence may rather point towards a lack of beach ridge preservation during this time. Such a lack could either be explained by a lack of sediment supply, a significant drop of sea level (at least some decimetres), or a time of highly fluctuating sea level. As there is no indication for a change in sediment supply or a reason to expect one, we favour sea-level drop as the controlling factor for the gap observed between the two sets of beach ridges.

The set of ridges located seaward (D, C, B) at the Chanthaburi estuary were deposited between ca. 2100 and 1200 yr ago, and coastal landforms with similar age have been documented in the vicinity of the study area (Chataro et al., 2022). While the information about the development of RSL change in the Gulf of Thailand and the neighbouring Sunda Shelf during this time is controversial (cf. Englong et al., 2019; Wan et al., 2020), some studies suggest it may have dropped by almost 1 m during this time (Tjia, 1996; Oliver and Terry, 2019). If these reconstructions are correct, a strong regression tendency may likely have caused the seaward migration of the beach ridges (Fig. 3B and C). With the formation of the beach ridges, the Chanthaburi
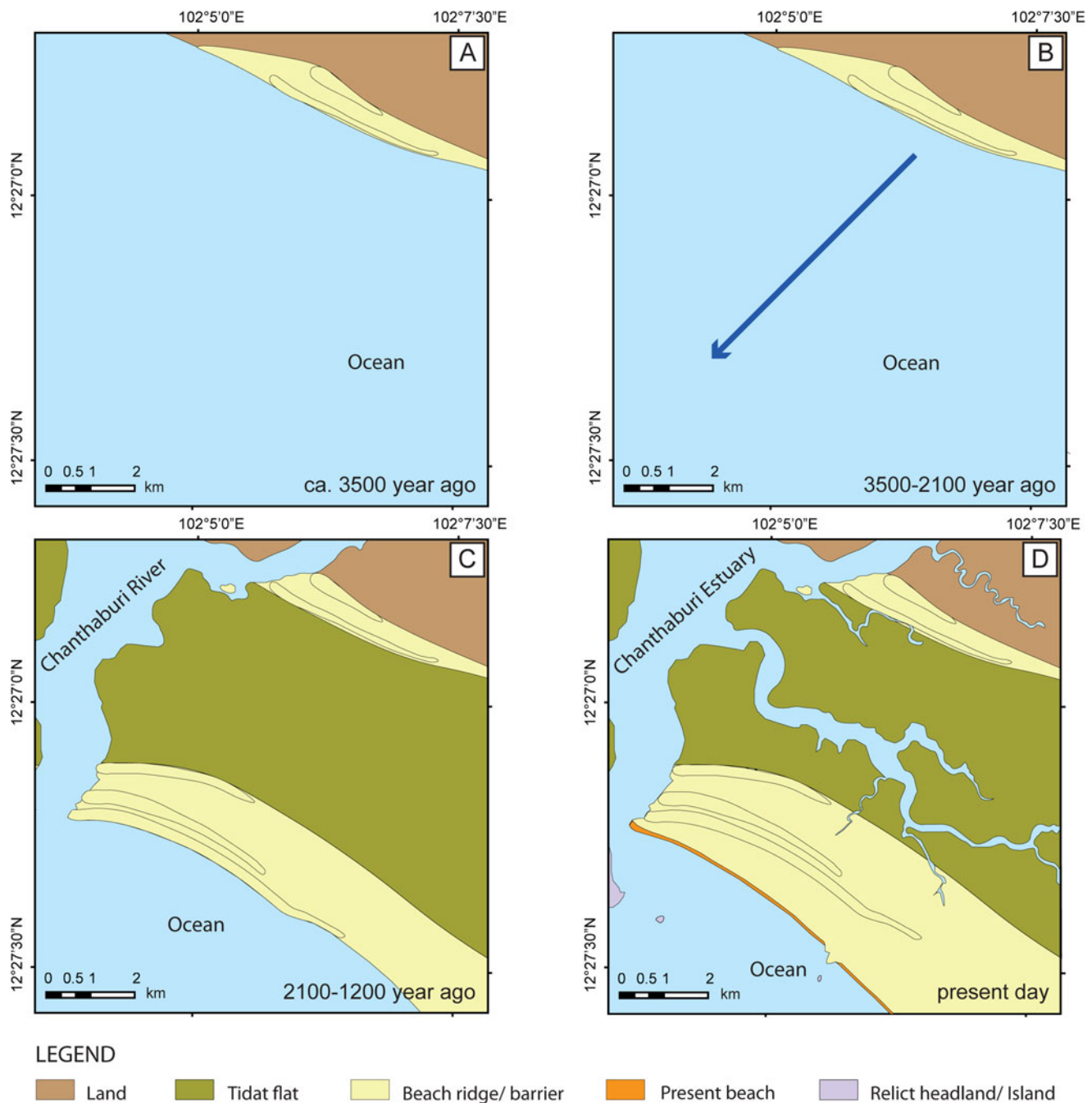
Figure 3. Schematic model of the coastal depositional environment evolution of Chanthaburi. (A) Around 3500 yr ago, a high sea-level position causes the development of beach ridges along the shoreline. (B) A substantial drop in sea level between 3500 and 2100 yr ago might be responsible for the lack of beach ridge formation during this time. (C) The seaward set of beach ridges establishes with falling sea level between ca. 2100 and 1200 yr ago and forms the bar-built Chanthaburi estuary. (D) Present-day coastal setting at Chanthaburi.

River as well as the nearby Welu River developed estuaries that are to be classified as barrier(-enclosed) or bar-built estuaries (cf., Roy et al., 1980; Hume and Herdendorf, 1988). Since the formation of ridge B some 1200 yr ago, the coastline position has apparently been rather stable, as this ridge is only some 100 m from the present beach ridge on the active coast (ridge A).

In contrast to our study, Mallinson et al. (2014) observe uniform progradation of a strandplain in the Setiu coastal region of NE Malaysia for the period ca. 3.0 to 1.9 ka and interpret this to reflect either constant slow relative sea-level fall or a still

stand. However, Woodroffe and Horton (2005) and Mann et al. (2019) imply that the exact knowledge of sea-level dynamics is poorly constrained for this period in SE Asia, and Surakiatchai et al. (2019) in fact summarise evidence of a steady sea-level lowering. Nevertheless, while a substantial sea-level drop could explain the observed lack of beach ridges along the Chanthaburi coast, it appears mandatory to collect more data from the wider region to either enforce or reject this hypothesis. One option to do so would be a geophysical survey to decipher the internal structure of beach ridges as well as drilling and investigating

sediments in the estuary zone, which is beyond the scope of the present study.

CONCLUSIONS

OSL dating of the landward set of beach ridges south of the Chanthaburi estuary reveals evidence for a higher sea level around 3500 yr ago. Possibly, this was followed by a substantial drop and potential subsequent rise of sea level between ca. 3500 and 2100 yr ago, responsible for the gap between the two sets of beach ridges later occupied by the Chanthaburi estuary tidal zone. The following slow retreat of sea level formed the seaward set of beach ridges between ca. 2100 and 1200 yr ago. Eventually, the modern beach ridge formed after this time.

REFERENCES

Abdulkarim, M., Grema, H.M., Adamu, I.H., Mueller, D., Schulz, M., Ulbrich, M., Miocic, J., Preusser, F., 2021. Effect of using different chemical dispersing agents in grain size analyses of fluvial sediments via laser diffraction spectrometry. *Methods and Protocols* **4**, 44.

Blott, S.J., Pye, K., 2001. GRADISTAT: a grain size distribution and statistics package for the analysis of unconsolidated sediments. *Earth Surface Processes and Landforms* **26**, 1237–1248.

Brill, D., Jankaew, K., Brückner, H., 2015. Holocene evolution of Phra Thong's beach-ridge plain (Thailand)—chronology, processes and driving factors. *Geomorphology* **245**, 117–134.

Charusiri, P., Clark, A.H., Farrar, E., Archibald, D., Charusiri, B., 1993. Granite belts in Thailand: evidence from the $^{40}Ar/^{39}Ar$ geochronological and geologic syntheses. *Journal of Asian Earth Sciences* **8**, 127–136

Chataro, C., Choowong, M., Phantuwongraj, S., 2022. Initial report on OSL dating from Pailin Beach Ridge Plain, Trat Province, eastern Gulf of Thailand with special highlight to record of the Holocene sea level change. *Bulletin of Earth Sciences of Thailand* **14**, 62–68.

Chen, M., Qi, H., Intasen, W., Kanchanapant, A., Wang, C., Zhang, A., 2020. Distributions of diatoms in surface sediments from the Chanthaburi coast, Gulf of Thailand, and correlations with environmental factors. *Regional Studies in Marine Science* **34**, 100991.

Choowong, M., 2002a. The geomorphology and assessment of indicators of sea-level changes to study coastal evolution from the Gulf of Thailand. In: *Proceedings of International Symposium on "Geology of Thailand."* Department of Mineral Resources, Thailand, pp. 207–220.

Choowong, M., 2002b. Coastal sedimentary lithofacies and episodic evolution from the Eastern part of Thailand. *Journal of Scientific Research Chulalongkorn University* **27**, 111–129.

Culver, S.J., Leorri, E., Mallinson, D.J., Reide Corbett, D., Shazili, N.A.M., 2015. Recent coastal evolution and sea-level rise, Setiu wetland, peninsular Malaysia. *Palaeogeography, Palaeoclimatology, Palaeoecology* **417**, 406–421.

Davies, J.L., 1957. The importance of cut and fill in the development of sand beach ridges. *Australian Journal of Science* **20**, 105–111.

Degering, D., Degering, A., 2020. Change is the only constant—time-dependent dose rates in luminescence dating. *Quaternary Geochronology* **58**, 101074.

[DMR] Department of Mineral Resources of Thailand, 2001. *Coastal Geomorphic Map of Amphoe Laem Sing-Amphoe Khao Saming, Chanthaburi (5433IV-5433I). 1:150,000.* Geological Survey Division, Bangkok.

[DMR] Department of Mineral Resources of Thailand, 2007. *Geological Map of Changwat Chanthaburi.* 1:250,000. Geological Survey Division, Bangkok.

Durand, Gaël, van den Broeke, M.R., Le Cozannet, G., Edwards, T.L., Holland, P.R., Jourdain, N.C., Marzeion, B., et al., 2022. Sea-level rise: from global perspectives to local services. *Frontiers in Marine Science* **8**, 709595.

Englong, A., Punwong, P., Selby, K., Marchant, R., Traiperm, P., Pumijumnong., N., 2019. Mangrove dynamics and environmental changes on Koh Chang, Thailand during the last millennium. *Quaternary International* **500**, 128–138.

Faye, S., Eynaud, F., Bosq, M., Lambert, C., Verdin, F., Vequaud, P., Lodyga, O., et al., 2019. Holocene palaeoenvironmental evolution of the Médoc peninsula (SW France): insights from the sedimentological study of the "Lède du Gurp" archaeological site. *Quaternaire* **30**, 31–46.

FitzGerald, D.M., Fenster, M.S., Argow, B.A., Buynevich, I.V., 2008. Coastal impacts due to sea-level rise. *Annual Review of Earth and Planetary Sciences* **36**, 601–647.

Galbraith, R.F., Roberts, R.G., Laslett, G.M., Yoshida, H., Olley, J.M., 1999. Optical dating of single and multiple grains of quartz from Jinmium Rock Shelter, Northern Australia: Part I, Experimental design and statistical models. *Archaeometry* **41**, 339–364.

Gouramanis, C., Switzer, A.D., Bristow, C.S., Pham, D.T., Mauz, B., Hoang, Q.D., Lam, D.D., et al., 2020. Holocene evolution of the Chan May coastal embayment, central Vietnam: changing coastal dynamics associated with decreasing rates of progradation possibly forced by mid- to late-Holocene sea-level changes. *Geomorphology* **367**, 107273.

Hanebuth, T.J.J., Stattegger, K., Grootes, P.M., 2000. Rapid flooding of the Sunda Shelf: a late-glacial sea-level record. *Science* **288**, 1033–1035.

Hanebuth, T.J.J., Voris, H.K., Yokoyama, Y., Saito, Y., Okuno, J., 2011. Formation and fate of depocenters on Southeast Asia's Sunda Shelf over the past sea-level cycle and biogeographic implications. *Earth-Science Reviews* **104**, 92–110.

Hansom, J., 2001. Coastal sensitivity to environmental change: a view from the beach. *Catena* **42**, 291–305.

Hara, H., Tokiwa, T., Kurihara, T., Charoentitirat, T., Ngamnithiporn, A., Visetnat, K., Tominaga, K., Kamata, Y., Ueno, K., 2018. Permian–Triassic back-arc basin development in response to Paleo-Tethys subduction, Sa Kaeo–Chanthaburi area in southeastern Thailand. *Gondwana Research* **64**, 50–66.

Heiri, O., Lotter, A.F., Lemcke, G., 2001. Loss on ignition as a method for estimating organic and carbonate content in sediments: reproducibility and comparability of results. *Journal of Paleolimnology* **25**, 101–110.

Hesp, P.A., Hung, C.C., Hilton, M., Ming, C.L., Turner, I.M., 1998. A first tentative Holocene sea-level curve for Singapore. *Journal of Coastal Research* **14**, 308–14.

Horton, B.P., Gibbard, P.L., Mine, G., Morley, R., Purintavaragul, C., Stargardt, J.M., 2005. Holocene sea levels and palaeoenvironments, Malay-Thai Peninsula, southeast Asia. *The Holocene* **15**, 1199–1213.

Hume, T.M., Herdendorf, C.E., 1988. A geomorphic classification of estuaries and its application to coastal resource management: a New Zealand example. *Ocean & Shoreline Management* **11**, 249–274.

Jacobs, Z., 2008. Luminescence chronologies for coastal and marine sediments. *Boreas* **37**, 508–535.

Jaroenongard, C., Babel, M.S., Shrestha, S., Weesakul, S., Nitivattananon, V., Khadka, D., 2021. Projecting relative sea level rise under climate change at the Phrachula Chomklao Fort tide gauge in the Upper Gulf of Thailand. *Water* **13**, 1702.

Kelsey, H.M., 2015. Geomorphological indicators of past sea levels. In: Shennan, I., Long, A.J., Horton, B.P. (Eds.), *Handbook of Sea-Level Research.* Wiley, Hoboken, NJ, pp. 66–82.

Kengkoom, S., 1992. Quaternary sea-level fluctuations in the coastal area of eastern Thailand: a synoptic view in relation to mineral resources exploration. *Journal of Southeast Asian Earth Sciences* **7**, 39–51.

Kongsen, S., Phantuwongraj, S., Choowong, M., Chawchai, S., Udomsak, S., Chansom, C., Ketthon, C., Surakiatchai, P., Miocic, J.M., Preusser, F., 2022. Multi-proxy approach to identify the origin of high energy coastal deposits from Laem Son National Park, Andaman Sea of Thailand. *Quaternary International* **625**, 82–95.

Lewis, S.L., Sloss, C.R., Murray-Wallace, C.V., Woodroofe, W.D., Smithers, S.C., 2013. Post-glacial sea-level changes around the Australian margin: a review. *Quaternary Science Reviews* **74**, 115–138.

Liu, S., Shi, X., Yang, G., Khokiattiwong, S., Kornkanitnan, N., 2016. Distribution of major and trace elements in surface sediments of the western Gulf of Thailand: implications to modern sedimentation. *Continental Shelf Research* **117**, 81–91.

Mallinson, D., Burdette, K., Mahan, S., Brook, G., 2008. Optically stimulated luminescence age controls on late Pleistocene and Holocene coastal lithosomes, North Carolina, USA. *Quaternary Research* **69**, 97–109.

Mallinson, D.J., Culver, S.J., Reide Corbett, D., Parham, P.R., Shazili, N.A.M., Yaaco, R., 2014. Holocene coastal response to monsoons and relative sea-level changes in northeast peninsular Malaysia. *Journal of Asian Earth Sciences* **91**, 194–205.

Mann, T., Bender, M., Lorscheid, T., Stocchi, P., Vacchi, M., Switzer, A., Rovere, A., 2019. Holocene sea levels in Southeast Asia, Maldives, India and Sri Lanka: the SEAMIS database. *Quaternary Science Reviews* **219**, 112–125.

Miocic, J.M., Sah, R., Chawchai, S., Surakiatchai, P., Choowong, M., Preusser, F., 2022. High resolution luminescence chronology of coastal dune deposits near Chumphon, western Gulf of Thailand. *Aeolian Research* **56**, 100797.

Murray, A.S., Wintle, A.G., 2000. Luminescence dating of quartz using an improved single-aliquot regenerative-dose protocol. *Radiation Measurements* **32**, 57–73.

Nielsen, A., Murray, A. S., Pejrup, M., Elberling, B., 2006. Optically stimulated luminescence dating of a Holocene beach ridge plain in northern Jutland, Denmark. *Quaternary Geochronology* **1**, 305–312.

Nimnate, P., Chutakositkanon, V., Choowong, M, Pailoplee, S., Phantuwongraj, S., 2015. Evidence of Holocene sea level regression from Chumphon coast of the Gulf of Thailand. *ScienceAsia* **41**, 55–63.

Oliver, G.J.H., Terry, J.P., 2019. Relative sea-level highstands in Thailand since the Mid-Holocene based on ¹⁴C rock oyster chronology. *Palaeogeography, Palaeoclimatology, Palaeoecology* **517**, 30–38.

Oliver, T.S., Murray-Wallace, C.V., Woodroffe, C.D., 2020. Holocene shoreline progradation and coastal evolution at Guichen and Rivoli Bays, southern Australia. *The Holocene* **30**, 106–124.

Oliver, T.S.N., Dougherty, A.J., Gliganic, L.A., Woodroffe, C.D., 2015. Towards more robust chronologies of coastal progradation: optically stimulated luminescence ages for the coastal plain at Moruya, south-eastern Australia. *Holocene* **25**, 536–546.

Oliver, T.S.N., Thom, B.G., Woodroffe, C.D., 2017. Formation of beach-ridge plains: an appreciation of the contribution by Jack L. Davies. *Geographical Research* **55**, 305–320.

Oppenheimer, M., Glavovic, B.C., Hinkel, J., van de Wal, R., Magnan, A.K., Abd-Elgawad, A., Cai, R., et al., 2019. Sea level rise and implications for low-lying islands, coasts and communities. In: Pörtner, H.-O., Roberts, D.C., Masson-Delmotte, V., Zhai, P., Tignor, M., Poloczanska, E., Mintenbeck, K., et al. (Eds.), *IPCC Special Report on the Ocean and Cryosphere in a Changing Climate*. Cambridge University Press, Cambridge, pp. 321–445.

Otvos, E.G., 2000. Beach ridges—definitions and significance. *Geomorphology* **32**, 83–108.

Pailoplee, S., Charusiri, P., 2017. Analysis of seismic activities and hazards in Laos: a seismicity approach. *Earth Planets and Space* **61**, 1313–1325.

Pailoplee, S., Choowong, M., 2013. Probabilities of earthquake occurrences in mainland Southeast Asia. Arabian *Journal of Geosciences* **6**, 4993–5006.

Peltier, W.R., 2004. Global glacial isostasy and the surface of the ice-age Earth: the ICE-5 G (VM2) model and GRACE. *Annual Reviews of Earth Planetary Science* **32**, 111–149.

Phoosongsee, J., Morely, C.K., 2019. Evolution of a major extensional boundary fault system during multi-phase rifting in the Songkhla Basin, Gulf of Thailand. *Journal of Asian Earth Sciences* **172**, 1–13.

Plater, A. J., Kirby, J. R., 2011. Sea-level change and coastal geomorphic response. In: Flemming, B.W., Hansom, J.D. (Eds.), *Treatise on Estuarine and Coastal Science*. Vol. 3. Elsevier, Amsterdam, pp. 39–72.

Prescott, J. R., Hutton, J. T., 1994. Cosmic ray contributions to dose rates for luminescence and ESR dating: large depths and long-term time variations. *Radiation Measurements* **23**, 497–500.

Preusser, F., Kasper, H.U., 2001. Comparison of dose rate determination using high-resolution gamma spectrometry and inductively coupled plasma-mass spectrometry. *Ancient TL* **19**, 19–23.

Rodrigues, K., Stapor, F.W., Rink, W.J., Dunbar, J.S., Doran, G., 2022. A 5700-year-old beach-ridge set at Cape Canaveral, Florida, and its implication for Holocene sea-level history in the southeastern USA. *The Holocene* **32**, 40–56.

Roy, P.S., Thom, B.G., Wright, L.D., 1980. Holocene sequences on an embayed high-energy coast: an evolutionary model. *Sedimentary Geology* **26**, 1–19.

Santisteban, J.I., Mediavilla, R., López-Pamo, E., Dabrio, C.J., Blanca Ruiz Zapata, M., José Gil García, M., Castaño, S., Martínez-Alfaro, P.E., 2004. Loss on ignition: a qualitative or quantitative method for organic matter and carbonate mineral content in sediments? *Journal of Paleolimnology* **32**, 287–299.

Scheffers, A. Brill, D. Kelletat, D. Brückner, H., Scheffers, S., Fox, K., 2012. Holocene sea levels along the Andaman Sea coast of Thailand. *The Holocene* **22**, 1169–1180.

Scoffin, T.P., Le Tissier, M.D.A., 1998. Late Holocene sea level and reef-flat progradation, Phuket, south Thailand. *Coral Reefs* **17**, 273–276.

Shawler, J.L., Hein, C.J., Obara, C.A., Robbins, M.G., Huot, S., Fenster, M.S., 2021. The effect of coastal landform development on decadal-to millennial-scale longshore sediment fluxes: evidence from the Holocene evolution of the central mid-Atlantic coast, USA. *Quaternary Science Reviews* **267**, 107096.

Short, A.D., Hesp, P.A., 1982. Wave, beach and dune interactions in southeast Australia. *Marine Geology* **48**, 259–284.

Sinsakul, S., 1992. Evidence of Quaternary sea level changes in the coastal areas of Thailand: a review. *Journal of Southeast Asian Earth Sciences* **7**, 23–37.

Sinsakul, S., Sonsuk, M., Hasting, P.J., 1985. Holocene sea levels in Thailand: evidence and basis for interpretation. *Journal of the Geological Society of Thailand* **8**, 1–12.

Sojisuporn, P., Sangmanee, C., Wattayakorn, G., 2013. Recent estimate of sea-level rise in the Gulf of Thailand. *Maejo International Journal of Science and Technology* **7**, 106–113.

Somboon, J.R.P., 1988. Paleontological study of the recent marine sediments in the lower central plain, Thailand. *Journal of Southeast Asian Earth Sciences* **2**, 201–210.

Somboon, J.R.P., Thiramongkol, N., 1992. Holocene highstand shoreline of the Chao Phraya delta, Thailand. *Journal of Southeast Asian Earth Sciences* **7**, 53–60.

Sone, M., Metcalfe, I., Chaodumrong, P., 2012. The Chanthaburi terrane of southeastern Thailand: stratigraphic confirmation as a disrupted segment of the Sukhothai Arc. *Journal of Asian Earth Sciences* **61**, 16–32.

Stattegger, K., Tjallingii, R., Saito, Y., Michelli, M., Thanh, N.T., Wetzel, A., 2013. Mid to late Holocene sea-level reconstruction of southeast Vietnam using beachrock and beach-ridge deposits. *Global and Planetary Change* **110**, 214–222.

Suk-ueng, N., Buranapratheprat, A., Gunbua, V., Leadprathom, N., 2013. Mangrove composition and structure at the Welu Estuary, Khlung District, Chanthaburi Province, Thailand. *Journal of Environmental Science, Toxicology and Food Technology* **7**, 17–24.

Surakiatchai, P., Choowong, M., Charusiri, P., Charoentitirat, T., Chawchai, S., Pailoplee, S., Chabangborn, A., et al., 2018. Paleogeographic reconstruction and history of the sea level change at Sam Roi Yot national park, Gulf of Thailand. *Tropical Natural History* **18**, 112–134.

Surakiatchai, P., Songsangworn, E., Pailoplee, S., Choowong, M., Phantuwongraj, S., Chabangborn, A., Charusiri, P., 2019. Optically stimulated luminescence dating reveals rate of beach ridge and sand spit depositions from the upper Gulf of Thailand. *Songklanakarin Journal of Science and Technology* **41**, 1136–1145.

Tamura, T., 2012. Beach ridges and prograded beach deposits as palaeoenvironment records. *Earth-Science Reviews* **114**, 279–297.

Tamura, T., Saito, Y., Bateman, M.D., Nguyen, V.L., Ta, T.K.O., Matsumoto, D., 2012. Luminescence dating of beach ridges for characterizing multi-decadal to centennial deltaic shoreline changes during Late Holocene, Mekong River delta. *Marine Geology* **326–328**, 140–153.

Terry, J. P., Goff, J., Jankaew, K., 2018. Major typhoon phases in the upper Gulf of Thailand over the last 1.5 millennia, determined from coastal deposits on rock islands. *Quaternary International* **487**, 87–98.

Thai Meteorological Department, 2020. Statistical Records of Tropical Cyclones Entering Thailand over 69 Years (1951–2019). Technical Report. [In Thai.] Bangkok.

Tjia, H.D., 1996. Sea-level changes in the tectonically stable Malay-Thai Peninsula. *Quaternary International* **31**, 95–101.

Trisirisatayawong, I., Naeije, M., Simons, W., Fenoglio-Marc, L., 2011. Sea level change in the Gulf of Thailand from GPS-corrected tide gauge data and multi-satellite altimetry. *Global and Planetary Change* **76**, 137–151.

Uchida, E., Nagano, S., Niki, S., Yonezu, K., Saitoh, Y., Shin, K.C., Hirata, T., 2022 Geochemical and radiogenic isotopic signatures of granitic rocks in Chanthaburi and Chachoengsao provinces, southeastern Thailand: implications for origin and evolution. *Journal of Asian Earth Sciences: X* **8**, 100111.

Vongvisessomjai, S., 2009. Tropical cyclone disasters in the Gulf of Thailand. *Songklanakarin Journal of Science and Technology* **31**, 213–227.

Wang, C., Chen, M., Qi, H., Intasen, W., Kanchanapant, A., 2020. Grain-size distribution of surface sediments in the Chanthaburi Coast, Thailand and implications for the sedimentary dynamic environment. *Journal of Marine Science and Engineering* **8**, 242.

Wan, J.X.W., Meltzner, A.J., Switzer, A.D., Lin, K., Wang, X.F., Bradley, S.L., Natawidjaja, D.H., Suwargadi, B.W., Horton, B.P., 2020. Relative sea level stability and the radiocarbon marine reservoir correction at Natuna Island, Indonesia, since 6400 yr BP. *Marine Geology* **430**, 106342.

Woodroffe, S.A., Horton, B.P., 2005. Holocene sea-level changes in the Indo-Pacific. *Journal of Asian Earth Sciences* **25**, 29–43.